Received: 24 March 2020 | Revised: 30 April 2020 | Accepted: 4 May 2020

DOI: 10.1002/term.3056

CLINICAL CASE STUDY

WILEY

Biomaterial and implant induced ossification: in vitro and in vivo findings

Pekka K. Vallittu[1] | Jussi P. Posti[2] | Jaakko M. Piitulainen[3] | Willy Serlo[4] | Jorma A. Määttä[5] | Terhi J. Heino[5] | Stefania Pagliari[6] | Stina M. Syrjänen[7] | Giancarlo Forte[6]

[1]Department of Biomaterials Science, Institute of Dentistry, University of Turku and City of Turku, Welfare Division, Turku, Finland

[2]Division of Clinical Neurosciences, Department of Neurosurgery, Turku Brain Injury Centre, Turku University Hospital and University of Turku, Turku, Finland

[3]Division of Surgery and Cancer Diseases, Department of Otorhinolaryngology - Head and Neck Surgery, Turku University Hospital, Turku Finland and University of Turku, Turku, Finland

[4]PEDEGO Research Unit, University of Oulu, Oulu, Finland and Department of Children and Adolescents, Oulu University Hospital, Oulu, Finland

[5]Institute of Biomedicine, University of Turku, Turku, Finland

[6]International Clinical Research Center of St. Anne's University Hospital Brno, Brno, Czech Republic

[7]Department of Oral Pathology and Radiology, Institute of Dentistry, University of Turku, Turku, Finland

Correspondence
Pekka Vallittu, Institute of Dentistry, University of Turku, Lemmikäisenkatu 2, FI-20520 Turku, Finland.
Email: pekka.vallittu@utu.fi

Giancarlo Forte, PhD, Center for Translational Medicine (CTM), International Clinical Research Center (ICRC), St. Anne's University Hospital, Studentska 6, Brno 62500, Czech Republic.
Email: giancarlo.forte@fnusa.cz

Abstract

Material-induced ossification is suggested as a suitable approach to heal large bone defects. Fiber-reinforced composite–bioactive glasses (FRC-BGs) display properties that could enhance the ossification of calvarial defects. Here, we analyzed the healing processes of a FRC-BG implant in vivo from the perspective of material-induced ossification. Histological analysis of the implant, which was removed 5 months after insertion, showed the formation of viable, noninflammatory mesenchymal tissue with newly-formed mineralized woven bone, as well as nonmineralized connective tissue with capillaries and larger blood vessels. The presence of osteocytes was detected within the newly generated bone matrix. To expand our understanding on the osteogenic properties of FRC-BG, we cultured human adipose tissue-derived mesenchymal stromal cells (AD-MSCs) in the presence of two different BGs (45S5 and S53P4) and Al_2O_3 control. AD-MSCs grew and proliferated on all the scaffolds tested, as well as secreted abundant extracellular matrix, when osteogenic differentiation was appropriately stimulated. 45S5 and S53P4 induced enhanced expression of COL2A1, COL10A1, COL5A1 collagen subunits, and pro-osteogenic genes BMP2 and BMP4. The concomitant downregulation of BMP3 was also detected. Our findings show that FRC-BG can support the vascularization of the implant and the formation of abundant connective tissue in vivo. Specifically, BG 45S5 and BG S53P4 are suited to evoke the osteogenic potential of host mesenchymal stromal cells. In conclusion, FRC-BG implant demonstrated material-induced ossification both in vitro and in vivo.

KEYWORDS

bioactive glass, bioactivity, biomaterial-induced ossification, cranial implant, fiber-reinforced composite, osteogenesis

Funding information
European Social Fund and European Regional Development Fund-Project MAGNET, Grant/Award Number: CZ.02.1.01/0.0/0.0/15_003/0000492

1 | INTRODUCTION

Ossification of large bone defects is still a prominent clinical challenge, although different kinds of implants have been introduced in the clinical pipeline. Implant material-induced ossification has been suggested to be the mechanism for inducing bone growth to heal large bone defects (Bohner & Miron, 2019). Recent studies suggested that osteoinduction by biomaterial occurs when a porous material allowing blood vessels ingrowth and the biomaterial mineralizes in vivo. One clinical indication where implant-induced ossification is beneficial is the repair of cranial defects by cranioplasty implants. A cranial bone defect can result from treatment of a traumatic brain injury or be caused by an infection, a congenital anomaly, or a tumor. The aim of cranioplasty surgery is to reconstruct the bone defect to physically protect the brain tissues, to retain a physiologic cerebral perfusion and pressure conditions, and to achieve an optimal cosmetic outcome post-surgery (Ashayeri, Jackson, Huang, Brem, & Gordon, 2016; Coelho et al., 2014; Di Stefano et al., 2016). Cranial bone defect repairs are based on autologous bone flaps and synthetic biomaterial implants. The present methods are not free of limitations: many autologous bone flaps are resorbed or infected, and synthetic materials also commonly show complications related to periprosthetic infections (Bobinski, Koskinen, & Lindvall, 2013; Coulter et al., 2014; Piitulainen et al., 2015). On the other hand, metallic implants may interfere with post-operative radiation therapy and cause artefacts in computer tomography (CT) and magnetic resonance imaging (MRI) (Rendenbach et al., n.d.; Cabraja, Klein, & Lehmann, 2009; Zanotti et al., 2016).

A fiber-reinforced composite–bioactive glass (FRC-BG) implant has been developed to mimic the lamellar structure of cortical bone, whereas its biomechanics and porous structure mimic cancellous bone (Aitasalo, Piitulainen, Rekola, & Vallittu, 2014; Nganga, Ylä-Soininmäki, Lassila, & Vallittu, 2011a; Peltola et al., 2012; Tuusa et al., 2008; Tuusa, Lassila, Matinlinna, Peltola, & Vallittu, 2005; Tuusa, Peltola, Tirri, Lassila, & Vallittu, 2007). The FRC-BG implant system is designed for orthopedic, cervical spine, and cranial surgeries—the latter clinical use being already approved (Vallittu, 2017). FRC-BGs have high fracture toughness with continuously oriented reinforcing glass fibers and a durable onlay implant structure. The sandwich structure allows incorporation of osteogenesis-enhancing filler particles into the implant. This effect has been documented in animal studies and clinically by positron emission tomography (PET) and radiological examinations (Vallittu, 2017). Out of the bioactive filler particles, silicate bioactive glasses (BGs) are used in surgery, when large, infected bone defects are augmented (Baino et al., 2019; Bjorkenheim et al., 2017; Bjorkenheim et al., 2019; Frantzen et al., 2011; Kankare & Lindfors, 2016; Rantakokko et al., 2012).

Based on the available in vitro and in vivo data, the function of the implant depends on two subsequent phenomena. First, the BG particles, which come into contact with the extracellular fluid, dissolve and release the loosely bonded glass network via rapid ion exchange with the H^+ from the fluid (Vallittu et al., 2015). The ion exchange furthermore leads to an increase in pH, thus making the environment bacteriostatic (Bigoni et al., 2019; Sarin et al., 2016; Zhang et al., 2010; Zhang, Hupa, & Hupa, 2008). The higher pH also drives the partial solubilization of the BG silica network, hence causing the release of silica as $Si(OH)_4$ into the fluid and resulting in the formation of silanols (Si-OH) at the BG particle and fiber-reinforced composite (FRC) surface. In the subsequent steps, calcium and phosphate from the extracellular fluid and from the bioactive glass first forms amorphous hydroxyapatite $Ca_{10}(PO_4)_6(OH)_2$, which then forms a carbonate-substituted hydroxyapatite layer on the implant surface. This makes the FRC surface osteoconductive.

Second, ion release is suggested to promote the osteogenic differentiation of mesenchymal stromal cells (MSCs) within and around the implant (Bjorkenheim et al., 2017; Bjorkenheim et al., 2019), similarly to other calcium phosphate-containing biomaterials (Nakamura et al., 2010; Schäck et al., 2013; Shih et al., 2014; Viti et al., 2016). Changes in the extracellular fluid pH are known to affect cell function, bone formation, and mineralization (Porgham Daryasari et al., 2019; Tan et al., 2018) and certain compositions of BGs (i.e., 45S5) can induce alkalization of a static, cell-free fluid microenvironment up to the level of pH 9.0. Even in the presence of cells, pH can reach the level of 8.0, at which no bone formation has been observed (Monfoulet et al., 2014). On the other hand, BG S53P4, which is used in the clinic in bone defect augmentation (Frantzen et al., 2011; Vallittu et al., 2015), has a lower dissolution rate, with pH remaining at the level of 7.8, even in a cell-free microenvironment (Vallittu et al., 2015).

Based on our previous radiological observations of FRC-BG implants with BG S53P4, bone formation was shown to occur next to *dura mater* even in large bone defects (Piitulainen, Posti, Vallittu, Aitasalo, & Serlo, 2019). In a preliminary histological evaluation of a removed FRC-BG implant, osteoblasts and maturing bone with blood vessels were found close to the BG particles (Kasir, Vernekar, & Laurencin, 2017). Although the osteogenic function of the FRC-BG implant is supported by several in vitro and in vivo studies, a deeper histological understanding of bone formation and the role of BGs in the implant-induced osteogenesis is needed.

Here, we analyzed the in vivo and in vitro processes of FRC-BG implant healing from the perspective of material-induced ossification. We first describe the histology of a large S53P4 FRC-BG implant, which was removed 5 months after implantation because of wound infection. The ground sections were immunohistochemically stained

for various markers to gain a deeper insight into the expected implant osteogenesis and neovascularization. The implant surface was also examined to verify in vivo biomineralization by calcium phosphate. Finally, the ability of S53P4 and two other FRC-BG formulations (Al_2O_3 and 45S5) to support adipose-derived mesenchymal stromal cell (AD-MSC) adhesion, proliferation, and osteogenic differentiation was evaluated. This comparative study clarified how S53P4 and 45S5 BGs induce secretion of extracellular matrix (ECM) and evoke the osteogenic potential of host MSCs.

2 | MATERIALS AND METHODS

2.1 | Patient case

A 53-year-old man was diagnosed with epidermoid carcinoma (grade III, T4/N1/M0) of the esophagus in 2011. He underwent resection of the lower esophagus, but a few weeks after the procedure, he developed tiredness and clumsiness. Head MRI showed a frontal cerebral metastasis, which was completely removed 2 months after the first operation. Dura mater was intact, and there was no need to use any artificial material. An autologous bone flap was used to close the calvarial opening for tumor resection. However, the autologous bone implant was unsuccessful due to a refractory infection. The bone flap was removed, and the patient was considered eligible for cranioplasty in 2016. A custom made FRC-BG implant (Glace Implant™) with an area of 85 cm^2 was designed and manufactured by the Skulle Implants Corporation (Turku, Finland) and selected to cover the bone defect. Anatomical shape was based on the contralateral side of the skull model. The CT scan reconstruction and implant design are shown in Figure 1a.

In brief, the implant was a sandwich structure consisting of outer and inner surface glass FRC laminates with a polymer matrix of dimethacrylates. The outer and inner surface of the implant was FRC laminate with mesh pore diameter of 0.4 mm. The space between the outer and inner laminates was filled with BG particles (S53P4, BonAlive Biomaterials, Turku, Finland) of a particle size of 0.5 mm. FRC laminates were biostable, and the BG dissolved over time in vivo. The implant was designed as an onlay implant with a margin width of 10 mm and a thickness of 0.8 mm. The margin was perforated to receive fixation screws. The implant was sterilized by hydrogen peroxide plasma method (Sterrad, Johnsson and Johnsson, Irvine, CA).

After cranioplasty surgery, recurrent infections occurred during 5 months at the scalp wound area (detail of surgery and follow-up are described in Data S1). Hence, the removal of the implant was found to be necessary. The FRC-BG implant was removed and fixed in 80% ethanol for further histological examinations. Samples were cut with a diamond cutting disc and further processed for histological and immunohistochemical studies. An additional sample of the implant was investigated by scanning electron microscope and energy dispersive X-ray spectroscopy (SEM-EDS) to determine calcium and phosphate precipitation on the implant surface. The wound was directly closed, and the patient was left for healing and waiting for a new cranioplasty operation.

2.2 | Plastic embedding and ground sections for histology and IHC

The sample was first dehydrated using ethanol with a gradient of 70%, 96%, and finally 100% ethanol for 24 h, each at room temperature (RT). The sample was then defatted in xylene twice at

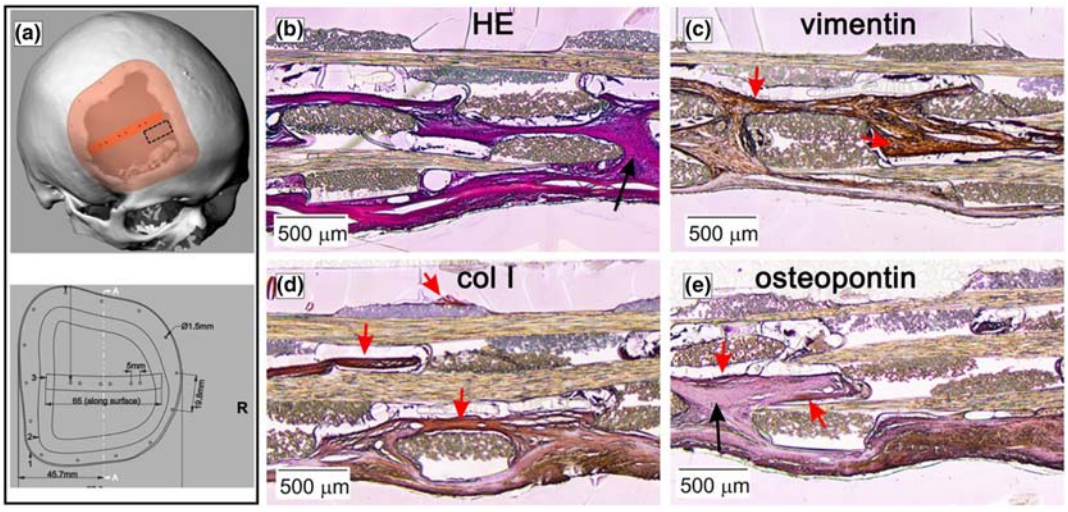

FIGURE 1 Fiber-reinforced composite (FRC) implant is surrounded by de novo produced tissue in vivo. (a) CT scan reconstruction of the bone defect (top) and design (bottom) of the FRC implant. (b) Hematoxylin/eosin staining of sections obtained from the implant. (c–e) Immunohistochemistry staining for the indicated proteins of sections obtained from the implant. The brown-colored areas indicate positive staining. Arrows identify osteocytes buried within the bone matrix. Original magnification is ×25 [Colour figure can be viewed at wileyonlinelibrary.com]

RT for 24 h before embedding in the low-temperature embedding system based on methyl methacrylate (Technovit 9100 New® (Heraeus Kulzer GmbH, Germany). The infiltration in Technovit 9100 New® solutions was done as follows: Xylene/Technovit 9100 New® basic solution at RT for 24 h followed by pre-infiltration in Solution 1 at RT for 24 h, then pre-infiltration in Solution 2 at 4°C for 24 h, followed by the final infiltration solution at 4°C for 24 h. After polymerization, sample blocks were cut perpendicular to the long bone axis and to the depth of the implant by using a diamond disc. After grinding, the cutting area was polished by P4000 grit sandpaper. A Superfrost Plus slide (Erie Scientific, Portsmouth, NH) was glued with Technovit 7210 VLC Precision adhesive (Kulzer) to the polished side of the block with ultraviolet (UV)-light. The second cut incision was made approximately 100 μm from the slide and simultaneously parallel with the slide. The slide with the section was then grinded using a sequence of abrasive papers (P800, P1200, and P2500 grit) to a final thickness of approximately 20 μm. The sections were dried overnight at 50°C and then immersed in MEA (1-acetoxy-2-methoxy-ethane) for 2 × 30 min followed by xylene 2 × 5 min, then through a graded ethanol series (absolute ethanol, 96%, 70%, 50%, 20% ethanol, and finally water) for 5 min each. These sections were used for hematoxylin–eosin staining according to the routine procedures for immunohistochemical studies.

2.3 | Immunohistochemistry

The immunohistochemical staining was carried out by using the immunoperoxidase detection method with the following primary antibodies and dilutions: vimentin, 1:150 (monoclonal, Dako #M7020); collagen I, 1:100 (polyclonal, Abbiotec #251221); osteopontin (OPN) 1:100 (monoclonal, Epitomics, #AC-0102RUO); CD31, 1:30 (monoclonal, Dako, #M0823), and IGF1 dilution at 10 μg/ml (polyclonal, Lifespan BioSciences #LS-C388624). For antigen retrieval, the sections were pretreated with 0.05% trypsin at 37°C for 15 min, except for CD31 and IGF1, where antigen retrieval was performed by microwave boiling in citrate buffer, pH 6.0. All sections were incubated with primary antibodies overnight at 4°C. The Dako REAL Detection System Peroxidase/DAB+, Rabbit/Mouse kit (Dako, #K5001) was used according to the manufacturer's instructions.

2.4 | Scanning electron microscopy and energy-dispersive X-ray spectroscopy

Cell colonization on the FRC scaffold surface was examined after 21 days using a scanning electron microscope (SEM). The samples were washed three times for 10 min in cacodylate buffer, dehydrated via an ethanol series (10%–100%) for 10 min per incubation and then stored at 4°C until being transferred for drying and coating. Dried samples were fixed on holders with carbon tape, sputter-coated with platinum (JFC-1300 autofine coater—JEOL, 151 40 mA, 15 s) and visualized under a JCM-6000 benchwork SEM (JEOL). This process was done under high-vacuum, using a SEI detector PC-standard, with an accelerating voltage of 10 kV.

Two samples of the implant were taken for SEM-EDS analysis (same region as for histology and immunohistochemistry [IHC]). Eight spot measurements of the samples were carried out with 15 kV accelerating voltage by using BSD Full Detector (PhenomWorld PW-100-017, The Netherlands) for determining calcium and phosphorus atomic concentration ratio.

2.5 | FRC scaffolds for in vitro osteogenesis studies

FRC scaffolds for the in vitro osteogenesis experiments had the same structural design and FRC material, polymerization process, and sterilization as the implant used for the patient. Specimens were 10.0 × 10.0 mm in size and had a thickness of 1.0 mm at the center where the filler particles were incorporated. The scaffold surface was a mesh-like laminate with a pore size of 0.4 mm in diameter (Figure S1). The space between the outer and inner laminates was filled with particles of BG S53P4 (wt%-composition: SiO_2: 53%; Na_2O 23%; CaO 20%, P_2O_5 4%, BonAlive Biomaterials, Turku, Finland) or BG 45S5 (wt-% composition: SiO_2: 45%; Na_2O: 24.5; CaO 24.5; P_2O_5: 6%; Mo-Sci, Rolla, MO, USA) of a particle size of 500 μm. Inert control particles were alumina (Al_2O_3; Mo-Sci, Rolla, MO, USA). Scaffold weight was 100 mg, and filler fraction was 30 wt%. In the experiments, 20 scaffolds were used per group.

2.6 | Cultures of AD-MSCs on FRC scaffolds

hTERT immortalized AD-MSCs (ASC52telo, ATCC® SCRC-4000™) were purchased from American Type Culture Collection (ATCC, Manassas, VA, USA). The cells were cultured in Dulbecco's modified Eagle's medium with 4.5 g/L Glucose (DMEM high Glucose, Lonza) supplemented with 10% fetal bovine serum (FBS), 2-mM L-glutamine and 100-U/ml penicillin/streptomycin (growth medium). Sterile FRC scaffolds were transferred to ultra-low attachment plates (Corning, New York, NY, USA) and preconditioned with growth medium. Cells were harvested after 24 h, counted and seeded at the density of 10×10^6 cells/cm^2 onto FRC scaffolds, either in growth medium or in osteogenic differentiation medium (Human Mesenchymal Stem Cell Osteogenic medium, Lonza, Basel, Switzerland), and cultured for 21 days. Osteogenic differentiation was assessed after 14 days of culture by Alizarin Red S (Sigma-Aldrich) staining and visualized under a light microscope. Control AD-MSCs were cultured on standard tissue culture polystyrene (TCPS).

2.7 | FACS analysis

For cell proliferation analysis, the cells were harvested from FRC scaffolds or TCPS on Day 3 or on Day 21 of culture by incubating for 10 min in 0.05% trypsin, 0.02% EDTA in phosphate-buffered solution

(PBS). The cells were then incubated for 60 min with anti-Ki67-AlexaFluor 488 (ABCAM, Cambridge, UK) and washed twice with ice-cold PBS. Cells were fixed in buffered 1% paraformaldehyde (PFA), 2% FBS for 15 min at 4°C and percentage of Ki67-positive cells was analyzed by BD FACS Canto II and plots prepared using FlowJo software v10 (Tree Star, Ashland, OR, USA).

2.8 | Analysis of FRC scaffold colonization by AD-MSCs

Cell colonization on the FRC scaffold surface was examined after 21 days using a SEM. Briefly, FRC scaffolds were cultured for 21 days with AD-MSCs previously incubated with the viable red fluorescent dye Vybrant DiI (Molecular Probes, Invitrogen, CA, USA) following the manufacturer's instructions. For osteogenic differentiation analysis, AD-MSCs were cultured onto the FRC scaffolds in differentiation medium (Lonza) for 14 days. At the given time-points, cells were washed twice with PBS and then switched to 1% PFA. Nuclei were counterstained with DAPI (Sigma-Aldrich) and 3D reconstruction of the colonized scaffolds obtained by Carl Zeiss LSM 7 MP Multiphoton Microscope.

2.9 | Quantitative real-time PCR

AD-MSCs were grown for 48 h on FRC scaffolds and total RNA extracted using a High Pure RNA Isolation Kit (Roche, Basel Switzerland), according to the manufacturer's instructions. Then, 500 ng of total RNA was transcribed into complementary DNA (cDNA) using an RT^2 First Strand Kit (QIAGEN, Hilden, Germany) and loaded on Osteogenesis RT^2 Profiler polymerase chain reaction (PCR) Array plates (PAHS-026Z, Qiagen). The quantitative PCR (qPCR) procedure was performed on a LightCycler 480 Real-Time PCR System (Roche), using the following program: 1 cycle at 95°C for 10 min; 45 cycles at 95°C for 15 s and 60°C for 1 min. Ct values were analyzed using Qiagen on-line platform, using *GAPDH*, *RPLO*, and *B2M* for normalization. The experiments were repeated in quadruplicate.

3 | RESULTS

FRC-BG (S53P4) is osteoconductive and induces neovascularization in vivo.

Hematoxylin/eosin staining showed newly-formed tissue inside and underneath the removed implant but not on the surface (Figure 1b). The newly-formed tissue appeared to be viable, non-inflammatory and of mesenchymal origin, as confirmed by vimentin positive staining by IHC (Figure 1c). Abundant staining for collagen I (Figure 1d) and osteopontin (Figure 1e) demonstrated the presence of ECM both inside the implant and especially underneath it, whereas no debris or particles released from the implant were observed.

A higher magnification of the implant sample showed both woven bone (Figure 2a) and lamellar bone (Figure 2b,c). The lamellar bone structure was well-organized and intensively positive for collagen I (Figure 2d,e). The bone surface was covered by osteoblasts (Figure 2c, f), whereas osteocytes were located deeper in the lamellar bone (Figure 2c). Strong immunopositivity for osteopontin was detected as a further evidence of active osteoblastic function and direct bone integration of the implant material (Figure 2g–i). No signs of inflammation or foreign body reaction were seen at this junction area.

The newly-formed tissue was heavily vascularized, as CD31 staining clearly identified pervious blood vessels close to the implant (Figure 3a). Additionally, osteocytes could be found in the proximity of neovascular units (Figure 3b–c).

SEM-EDS analysis of the implant material showed calcium phosphate precipitation isles on the implant surface with a Ca/P ratio of 1.67 (min 1.19, max 2.38). SEM examination showed also areas of glass fibers and polymer matrix where mineralization has not formed visible layers of calcium phosphate (Figure 4).

3.1 | AD-MSCs colonize FRC scaffolds and differentiate to mineralizing cells

For comparison, the adhesion and colonization capacity of AD-MSCs cultured onto different FRC scaffolds containing either S53P4, 4S5S, or Al2O3 as filler material was analyzed. Furthermore, their capacity to proliferate and differentiate into osteoblasts in the presence of induction medium was tested. Two-photon microscopy of AD-MSCs stained for Vybrant DiI dye and DAPI showed that the cells were indeed able to colonize the external walls of the FRC scaffolds (Figure 5a). After 21 days of culturing, the cells aligned and deposited abundant ECM on all the scaffolds tested (Figure 5b).

More importantly, AD-MSCs were shown to penetrate the inner core of the scaffolds (Figure 5c). FACS analysis of Ki67 proliferation marker in AD-MSCs showed that on Day 3 of cell culture on TCPS, 52% of the gated cells were positive for the Ki67 proliferation marker, which is remarkably higher than of those cells cultured with bioactive glass S53P4 (21.5%) or inert Al_2O_3 (25%; Figure 5d). However, on Day 21, the proportion of Ki67-positive of cells on S53P4 and Al_2O_3 scaffolds increased to 43.7% and 36.8%, respectively.

AD-MSCs grown on FRC scaffolds were also cultured in osteogenic medium for 21 days. Cells grown in osteogenic medium were able to fully colonize the scaffolds, similarly as in basal growth medium (see Figure 5). Differentiated cells deposited abundant ECM, which was found to cover the whole scaffold structure (Figure 6a) and showed successful mineralization on all three scaffolds, as demonstrated by Alizarin red staining (Figure 6b).

The osteogenic ability of AD-MSCs cultured on scaffolds with three different types of BG fillers was assessed by real-time qPCR (RT-qPCR) array (PAHS-026Z, Qiagen; Figure 6c). The analysis demonstrated that, although the three formulations of BG fillers were all able to support AD-MSC osteogenic differentiation, 45S5 induced the most pronounced upregulation of pro-osteogenic messenger RNAs

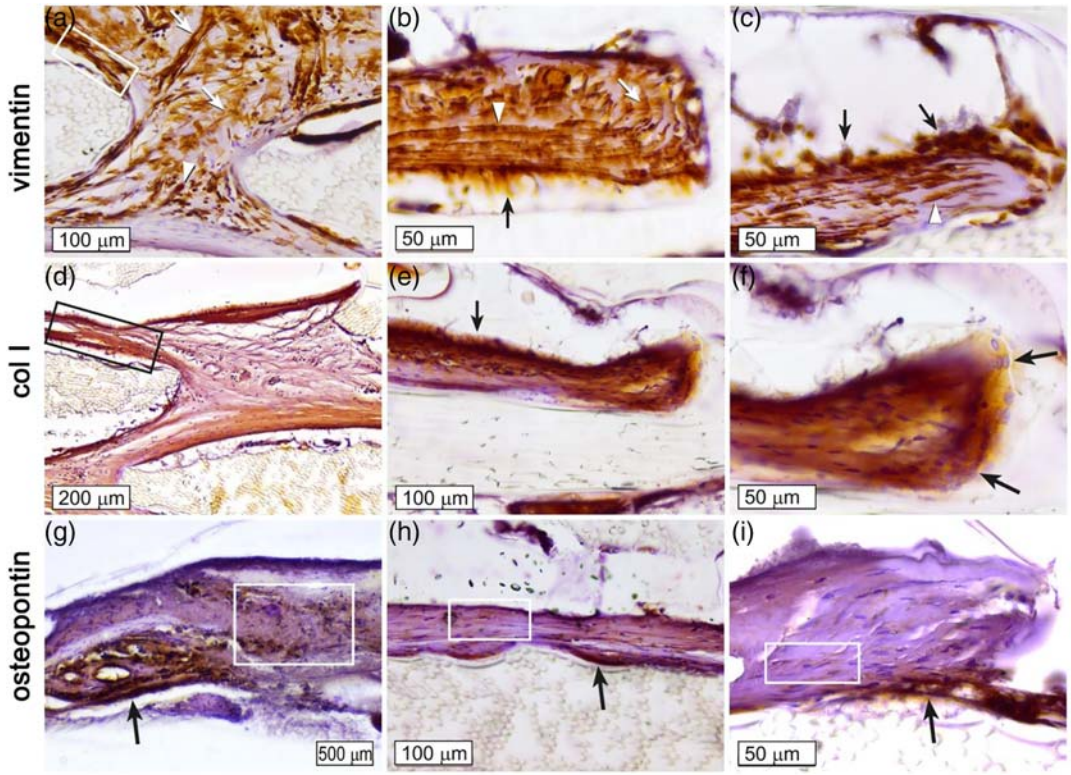

FIGURE 2 Fiber-reinforced composite (FRC) implant induces extracellular matrix (ECM) deposition and new bone formation. Immunohistochemistry (IHC) staining of the implant sections: (a) vimentin staining pattern identifies mesenchymal cells and structured fibers in proximity of the implant. White box: intense lamellar positivity is found adjacent to the implant material (Original magnification ×200). (b) Layered or lamellar configuration of early forming bone (white arrow head and arrow, respectively) showing also the Sharpey's fibers (black arrow). Original magnification ×400. (c) Osteoblasts (black arrows) on the surface of the mesenchymal tissue, with vimentin-positive lamellar structures within the newly formed tissue (white arrowhead). Original magnification ×400. (d) Black box: dense layers of collagen type I are seen in close proximity of the implant. Less intense and diffusely scattered staining for collagen I in the newly formed tissue between the two implant material layers (original magnification ×100). (e and f) Sharpey's fibers predominantly composed of type I collagen (black arrows; (e) and (f), original magnification ×200 and ×400, respectively). (g) Osteopontin staining in the newly-formed tissue adjacent to the implant tissue. White box: more scattered pattern is found deeper within the mesenchymal tissue. A dense osteopontin layer is also present adjacent to the implant material (black arrow). Original magnification ×100. (h and i) White box: tiny deposits of osteopontin are also found within the vimentin positive layers (similar position as white arrowhead in panel (c); (h) and (i), original magnification ×200 and ×400, respectively). [Colour figure can be viewed at wileyonlinelibrary.com]

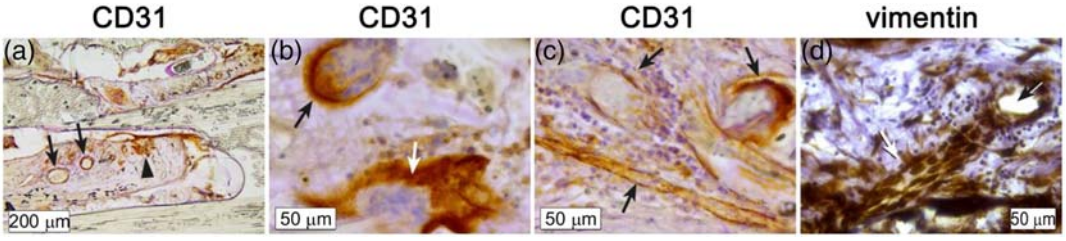

FIGURE 3 Vascularization of the newly-formed tissue surrounding the implant. (a) Vascular structures surrounded by a regular monolayer of CD31-positive endothelial cells (arrows) as well as areas of neovascularization (arrowhead) in the newly-formed tissue adjacent to the implant. Original magnification ×100. (b) Intense CD31 immunopositivity in the close proximity of pre-osteoblasts/osteoblasts in the newly-formed tissue. Original magnification ×400. (c) Newly-formed pervious capillaries, either longitudinally or transversally sectioned, as detected by CD31 positive staining. Original magnification ×400. (d) Vimentin staining of a newly-formed vessel adjacent to the implant. Original magnification ×400 [Colour figure can be viewed at wileyonlinelibrary.com]

(mRNAs) BMP2, BMP4, and BMP5 and concomitant downregulation of negative regulator BMP3 mRNA. In cells cultured within S53P4 scaffold, the expression of BMPs was slightly lower than in those cultured with 45S5 scaffold but still much higher than in those cultured with Al2O3 scaffold. Cell cultures on S53P4 and 45S5 formulations had both reduced expression of mRNA of anti-osteogenic

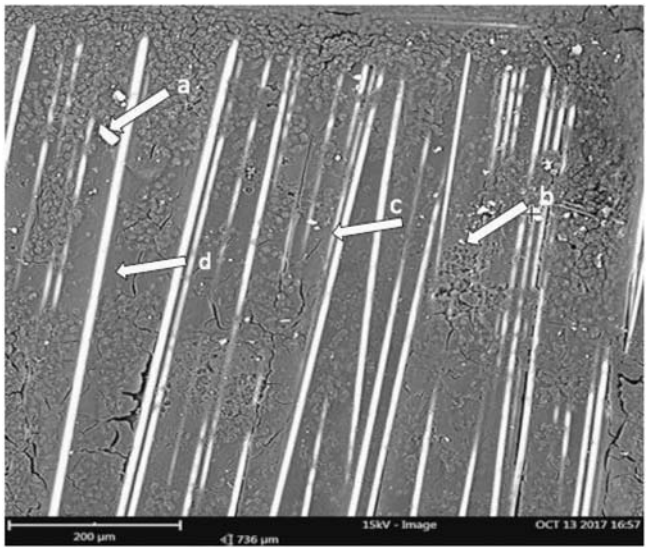

FIGURE 4 Scanning electron microscope (SEM) micrograph of the fiber-reinforced composite (FRC) surface of the implant after removal. (a) Precipitation of calcium phosphate crystals, (b) larger precipitation areas, (c) exposed glass fibers, and (d) polymer matrix of the FRC (bar 200 μm)

BMP5 when compared with AD-MSCs differentiated in the presence of an Al_2O_3 scaffold (Figure 6d). A slight, nonsignificant increase in the expression of IGF1/IGF1R axis could be detected on S53P4 (Figure 6d). Both 45S5 and S53P4 formulations induced the upregulation of genes encoding for collagen subunits (*COL2A1*, *COL10A1*, and *COL5A1*).

4 | DISCUSSION

In the present study, we investigated the healing process of FRC-BG implant in a large calvarial defect due to cranioplasty surgery. The implant, which had been functional for 5 months, had to be removed because of recurrent infections. Our analysis found that it was surrounded by numerous vimentin-positive mesenchymal cells, which were embedded in a mesh of collagen I and osteopontin, which is a protein known to modulate bone remodeling process, chemotaxis of inflammatory cells, and osteoblast responsiveness to extracellular stimuli (Kahles, Findeisen, & Bruemmer, 2014; Kusuyama et al., 2017). This demonstrates that the active ossification process had taken place as the expression of proteins in our samples reflected osteoblast differentiation, mineralization, and matrix maturation.

Detailed analysis of the explanted specimens allowed us to identify the presence of CD31-positive cells that highlighted the de novo formation of pervious vascular structures in the inner core and around the implant. Interestingly, S53P4 bioactive glass has been previously shown to increase the expression of vascular endothelial growth factor (VEGF) (Bjorkenheim et al., 2017), thus suggesting a potential mechanism behind our observation.

Porous structure of the scaffold and surface biomineralization in vivo by bioactive calcium phosphate, which are the key requirements for biomaterial-induced ossification, were fulfilled both with clinically used implant and in vitro FRC-BG scaffold. The semi-quantitative SEM-EDS examination of the implant showed calcium phosphate precipitate on the FRC implant surface with the 1.67 ratio of Ca/P, corresponding to the stoichiometric Ca/P ratio in hydroxyapatite. The osteo-conductivity of biomaterial implants can be increased by coating surfaces with calcium phosphate minerals (Ballo et al., 2008; Väkiparta et al., 2005) and the calcium and phosphorus precipitation of the substrate prior to osteoid synthesis is important for the osteo-conductivity of tissue-engineered scaffolds (Sautier et al., 1994). Additionally, in vitro experiments have previously confirmed that the FRC surface is mineralized with calcium phosphates in the presence of BG (Baino et al., 2019; Väkiparta et al., 2005). Thus, the previously described mechanisms by which BG releases ions to induce biomineralization in vitro and in vivo (Fagerlund, Hupa, & Hupa, 2013; Kasir et al., 2017; Nganga, Zhang, Moritz, Vallittu, & Hupa, 2012a; Posti et al., 2015; Ramesh, Tan, Hamdi, Sopyan, & Teng, 2004) were supported by the present study. When the implant-induced ossification of the in vivo FRC-BG implant is considered, the interaction between dura mater and cranial osteoblasts are important (Cowan et al., 2004; Mehrara et al., 1999). Taken together, it appears that for the peridural and intra-implant ossification, the role of dura mater and calcium phosphate mineralization surface are having a significant role (LeGeros, 2002).

The healing of a bone defect is a complex process controlled by several cell types and various molecular regulators. Activation of the healing process and formation of new bone begins by trauma-induced inflammation. In cranioplasty surgery, the bone margins of the defect are already healed at the time of implant placement, and thus, the activation of osteogenesis requires mechanical decortication of the bone margins. This causes extravasated blood to form a post-traumatic hematoma and to cause influx of cells, including inflammatory cells and MSCs. This is then followed by MSC differentiation and release of proteins for ECM deposition (Shiu, Leung, & Ko, 2018; Szcesny, 2018). In the case of the FRC-BG implant, the inner and outer surfaces of the implant were perforated, which enabled blood penetration and diffusion by capillary forces from the surgical site to cause instant hematoma throughout the implant (Nganga, Ylä-Soininmäki, Lassila, & Vallittu, 2011b; Nganga, Zhang, Moritz, Vallittu, & Hupa, 2012b).

We conducted an in vitro analysis of MSC osteogenic cell differentiation in the presence of different FRC compositions. The roles of BG S53P5 and 45S5 in osteogenic cell differentiation and osteogenesis have been previously studied. One of the key features of these materials is alkalinization of the environment by dissolution of the BG (Bjorkenheim et al., 2019). This is due to the consumption of protons (H_3O^+ ions) during the ion exchange reactions between the glass network and the aqueous media (Silver, Deas, & Erecinska, 2001; Vallittu et al., 2015). The BGs used in the FRC scaffolds of this study have a different dissolution profile: BG 45S5 dissolves faster than BG S53P5 and increases pH considerably more. The high alkalinization by BG

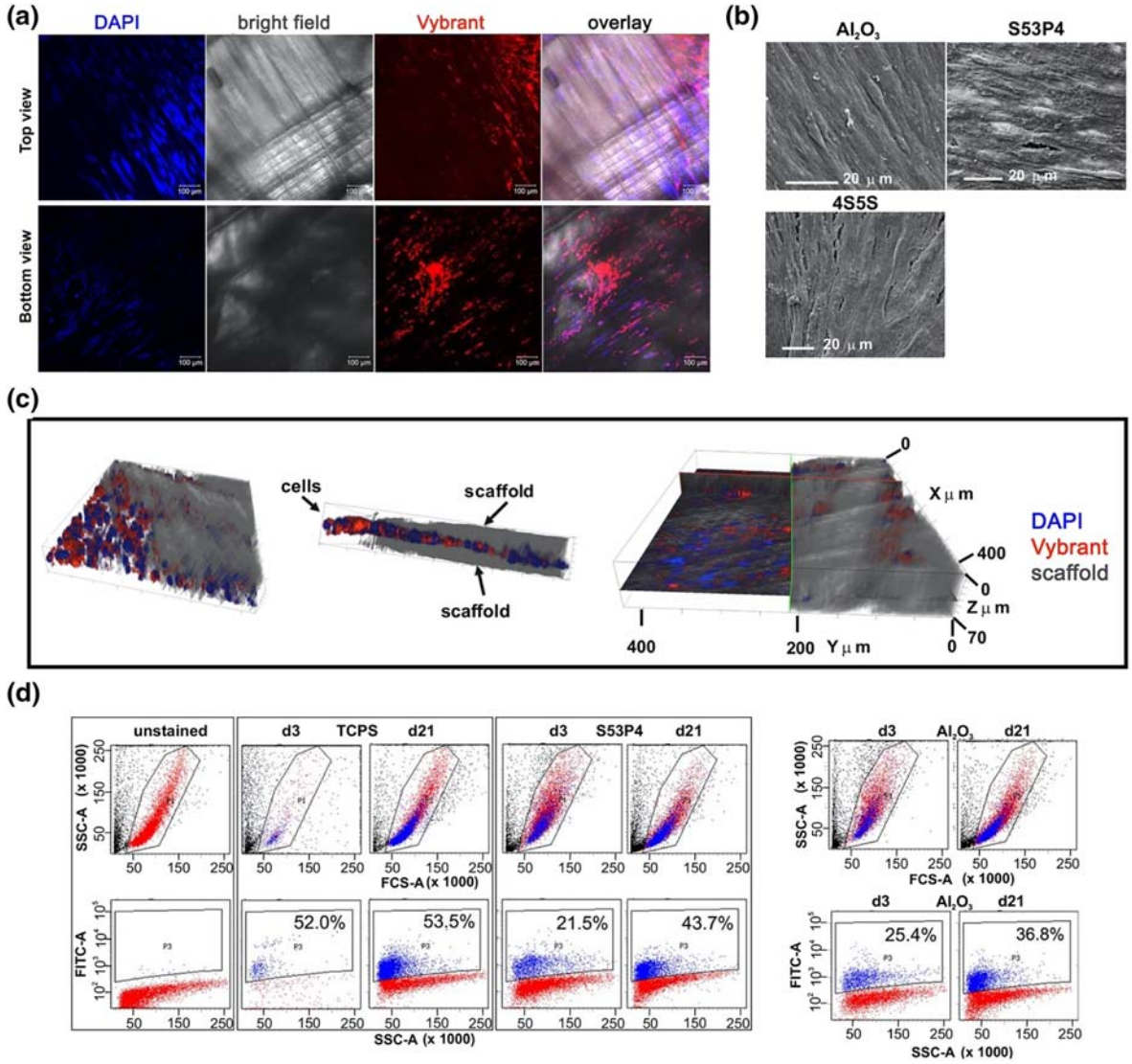

FIGURE 5 Adipose tissue-derived mesenchymal stem cells (AD-MSCs) colonize the fiber-reinforced composite (FRC) scaffolds. AD-MSCs were cultured on Al_2O_3, S53P4, and 4S5S scaffolds in basal growth medium for 21 days: (a) representative two-photon microscopy images of the top and bottom layers of S53P4 scaffolds cultured with AD-MSCs. Cells were stained for nuclei (DAPI, blue) and cytoplasm (Vybrant dye, red); (b) two-photon microscope 3D reconstruction of a representative section of S53P4 scaffold cultured with AD-MSCs for 21 days and stained as described above to demonstrate the colonization of the scaffold core by the cells; (c) representative scanning electron microscopy (SEM) images of AD-MSCs grown on the surface of the Al_2O_3, S53P4, or 4S5S scaffolds; (d) representative FACS dot plots depicting the expression of Ki67 proliferation marker in AD-MSCs cultured for 3 and 21 days on tissue culture polystyrene (TCPS) or on the indicated FRC scaffolds [Colour figure can be viewed at wileyonlinelibrary.com]

45S5 has been shown to inhibit MSC proliferation and differentiation, whereas a lower increase of pH at the presence of S53P4 did not demonstrate any inhibitory effects (Monfoulet et al., 2014; Vallittu et al., 2015). Although the pH changes in the FRC scaffolds used in this study were not measured, some significant observations on the osteogenic molecular patterns of AD-MSC differentiation were found. These could, in addition to the probable differences in the pH induced, be related to the release of calcium and phosphorus ions from the dissolving particles, which has been a phenomenon of interest in previous studies (Schäck et al., 2013; Shih et al., 2014). Ion release profiles of BG 45S5 and S53P4 have been determined, and it is known that in early stage dissolution of BG S53P4, the material releases somewhat higher quantities of phosphorus (PO_4^{3-}) than BG 45S5 (Nganga et al., 2012a).

We utilized an immortalized AD-MSC cell line that was previously proven effective in multilineage differentiation by our own group (Oliver-De La Cruz et al., 2019). For bone tissue engineering, many studies have compared the osteogenic capacity of human bone marrow derived MSCs (BM-MSCs) and AD-MSCs, and it is known that these two cell types have comparable characteristics with regards to cell morphology and surface marker expression profile (Shih et al., 2014). Some studies have, however, shown that AD-MSCs have increased osteogenic potential compared with BM-MSCs (Storm et al., 1994; Wang et al., 2014), which should be considered when

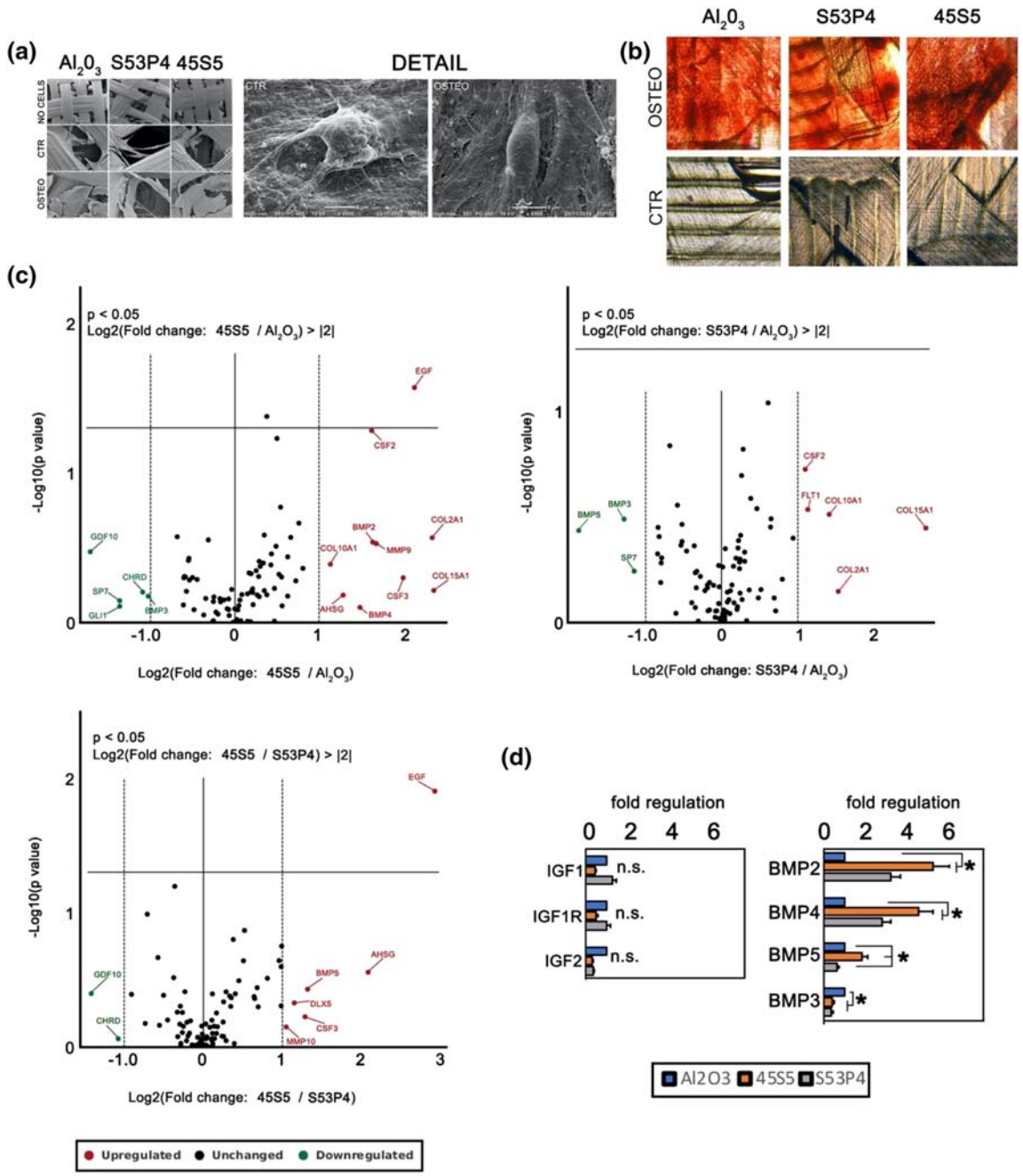

FIGURE 6 Adipose tissue-derived mesenchymal stem cells (AD-MSCs) acquire the osteogenic phenotype on fiber-reinforced composite (FRC) scaffolds. (a) Representative SEM images of the indicated FRC scaffolds alone (NO CELLS), in the presence of AD-MSCs (CTR) or in the presence of AD-MSCs stimulated with osteogenic medium (OSTEO, left). Representative scanning electron microscopy (SEM) images of single AD-MSCs cultured either in growth medium (CTR, center) or in osteogenic medium (OSTEO, right) for 14 days on S53P4 scaffold. Abundant extracellular matrix is seen surrounding the cells, and similar results were obtained on the other scaffolds. (b) Representative bright-field images of AD-MSCs cultured for 14 days in osteogenic (OSTEO, top line) or basal growth (CTR, bottom line) medium on the indicated FRC scaffolds and stained for Alizarin Red. (c) Volcano plot representing the genes involved in osteogenic differentiation being significantly regulated in AD-MSCs cultured for 48 h in osteogenic medium onto 45S5 or S53P4 as compared with Al_2O_3 scaffolds, as obtained by real-time quantitative polymerase chain reaction (RTq-PCR) array analysis. $n = 4$, $p < 0.05$. Red and green indicate up- and down-regulated genes, respectively. (d) Bar plot representation of the expression of selected genes involved in osteogenesis, as obtained by RTq-PCR array analysis. $n = 4$, $^{*}p < 0.05$ [Colour figure can be viewed at wileyonlinelibrary.com]

interpreting the results of this study. Experiments with FRC scaffolds and AD-MSCs demonstrated that although the three formulations of fillers were all able to support osteogenic differentiation, BG 45S5 induced a significant upregulation of BMP2 and BMP4, two master genes involved in promoting osteogenesis (De Ugarte et al., 2003) and the downregulation of BMP3, which is supposed to trigger bone

resorption. BMP2 is known to have a dose-dependent increase in bone regeneration (Cowan et al., 2007) which supports also our results obtained with AD-MSCs grown on BG S53P4 scaffolds. Also, AD-MSCs on S53P4 scaffolds showed a slight increase in the expression of IGF1/IGF1R, which could account for a superior performance in calvarial bone formation as suggested previously (Jiang et al., 2006). Both 45S5 and S53P4 formulations shared the upregulation of genes encoding for collagen subunits (*COL2A1*, *COL10A1*, and *COL5A1*), that are consistent with the substantial ECM deposition on the scaffolds.

In conclusion, FRG-BGs can support the vascularization of the implantation site and the deposition of abundant connective tissue from infiltrating cells. In the context of material-induced ossification, newly-formed bone with Sharpey's fibers and osteoblasts were found adjacent to the implant material, where Ca/P precipitation could be detected.

These results, as obtained from in vivo and in vitro experiments, support the conclusion that FRC-BG implant can trigger material-induced ossification.

In conclusion, we have demonstrated material-induced heterotopic ossification in FRG-BG material by histological and immunohistochemical examinations of an FRC-BG implant that had been *in situ* for 5 months. The results showed newly forming bone with Sharpey's fibers and osteoblasts adjacent to the implant material, where Ca/P precipitation was also found. The presence of capillaries and larger blood vessels was also demonstrated. AD-MSC model of in vitro osteogenesis revealed that when the scaffolds were loaded with BG 45S5 or S53P4, osteogenic differentiation was enhanced compared with the control filler of Al_2O_3. In summary, this study supports previous radiological findings of osteogenesis in FRC-BG implant healing.

ACKNOWLEDGEMENTS

Giancarlo Forte and Stefania Pagliari were supported by the European Social Fund and European Regional Development Fund-Project MAGNET (CZ.02.1.01/0.0/0.0/15_003/0000492). The study was supported by the BioCity Turku Biomaterials and Medical Device Research Program (www.biomaterials.utu.fi). FRC scaffolds for MSC tests were provided by Skulle Implants Corporation (www.skulleimplants.com).

Jussi P. Posti is supported by the Academy of Finland (grant #17379) and Pekka K. Vallittu and Jorma Määttä are supported by the Academy of Finland (grant #323596).

CONFLICT OF INTERESTS

Author Vallittu PK is a Member of the Board and shareholder of Skulle Implants Corp. Author Serlo W is a shareholder of Skulle Implants Corp.

ORCID

Pekka K. Vallittu https://orcid.org/0000-0002-9981-6717
Jussi P. Posti https://orcid.org/0000-0002-5925-5193
Jaakko M. Piitulainen https://orcid.org/0000-0001-9788-8904
Jorma A. Määttä https://orcid.org/0000-0001-8752-6862
Terhi J. Heino https://orcid.org/0000-0003-2274-6834
Stefania Pagliari https://orcid.org/0000-0003-2414-1468
Stina M. Syrjänen https://orcid.org/0000-0003-0738-5698
Giancarlo Forte https://orcid.org/0000-0002-1341-1023

REFERENCES

Aitasalo, K., Piitulainen, J. M., Rekola, J., & Vallittu, P. K. (2014). Craniofacial bone reconstruction with bioactive fibre composite implant. *Head and Neck*, *36*, 722–728. https://doi.org/10.1002/hed.23370

Ashayeri, K., Jackson, E. M., Huang, J., Brem, H., & Gordon, C. R. (2016). Syndrome of the trephined: A systematic review. *Neurosurgery*, *79*(4), 525–533. https://doi.org/10.1227/NEU.0000000000001366

Baino, F., Verne, E., Fiume, E., Peitl, O., Zanotto, O. D., Brandao, S. M., & Schellini, S. A. (2019). Bioactive glass and glass ceramic orbital implants. *International Journal of Applied Ceramic Technology*, *16*(5), 1850–1863. https://doi.org/10.1111/ijac.13236

Ballo, A. M., Kokkari, A. K., Mertetoja, V. V., Lassila, L. V., Vallittu, P. K., & Narhi TO. (2008). Osteoblast proliferation and maturation on bioactive fiber-reinforced composite surface. *Journal of Materials Science. Materials in Medicine*, *19*(10), 3169–3177. https://doi.org/10.1007/s10856-008-3453-y

Bigoni, M., Turati, M., Zanchi, N., Lombardo, A. S., Graci, J., Omeljaniuk, R. J., … Gaddi, D. (2019). Clinical applications of bioactive glass S53P4 in bone infections: Systematic review. *Eur Rev Med Phar Sci*, *23*, 240–251.

Bjorkenheim, R., Stromberg, G., Ainola, M., Uppstu, P., Aalto-Setala, L., Hupa, L., … Lindfors, N. (2019). Bone morphogenic protein expression and bone formation are induced by bioactive glass S53P4 scaffolds in vivo. *Journal of Biomedial Materials Research Part B Applied Biomaterials*, *107*(3), 847–857. https://doi.org/10.1002/jbm.b.34181

Bjorkenheim, R., Strömberg, G., Pajarinen, J., Ainola, M., Uppstu, P., Hupa, L., … Lindfors, N. C. (2017). Polymer-coated bioactive glass S53P4 increases VEGF and TNF expression in an induced membrane model in vivo. *Journal of Materials Science*, *52*(15), 9055–9065. https://doi.org/10.1007/s10853-017-0839-6

Bobinski, L., Koskinen, L.-O., & Lindvall, P. (2013). Complications following cranioplasty using autologous bone or polymethylmethacrylate-retrospective experience from a single center. *Clinical Neurology and Neurosurgery*, *115*(9), 1788–1791. https://doi.org/10.1016/j.clineuro.2013.04.013

Bohner, M., & Miron, R. J. (2019). A proposed mechanism for material-induced heterotopic ossification. *Materials Today*, *22*, 132–141. https://doi.org/10.1016/j.mattod.2018.10.036

Cabraja, M., Klein, M., & Lehmann, T.-N. (2009). Long-term results following titanium cranioplasty of large skull defects. *Neurosurgical Focus*, *26*, E10, 1–7. https://doi.org/10.3171/2009.3.FOCUS091

Coelho, F., Oliveira, A. M., Paiva, W. S., Freire, F. R., Calado, V. T., Amorim, R. L., … Teixeira, M. J. (2014). Comprehensive cognitive and cerebral hemodynamic evaluation after cranioplasty. *Neuropsych Disease and Treatment*, *10*, 695–701.

Coulter, I. C., Pesic-Smith, J. D., Cato-Addison, W. B., Khan, S. A., Thompson, D., Jenkins, A. J., … Mukerji, N. (2014). Routine but risky: A multi-centre analysis of the outcomes of cranioplasty in the Northeast of England. *Acta Neurochirurgica*, *156*, 1361–1368. https://doi.org/10.1007/s00701-014-2081-1

Cowan, C. M., Aghaloo, T., Chou, Y.-F., Walder, B., Zhang, X., Soo, C., … Wu, B. (2007). MicroCT evaluation of three-dimensional mineralization in response to BMP-2 doses in vitro and in critical sized rat calvarial defects. *Tissue Eng*, *13*(3), 501–512. https://doi.org/10.1089/ten.2006.0141

Cowan, C. M., Shi, Y.-Y., Aalami, O. O., Chou, Y.-F., Mari, C., Thomas, R., … Longaker, M. T. (2004). Adipose-derived adult stromal cells heal

critical-size mouse calvarial defects. *Nature Biotechnol*, *22*, 560–567. https://doi.org/10.1038/nbt958

De Ugarte, D. A., Morizono, K., Elbarbary, A., Alfonso, Z., Zuk, P. A., Zhu, M., … Benhaim, B. (2003). Comparison of multi-lineage cells from human adipose tissue and bone marrow. *Cells*, *Tissues*, *Organs*, *174*, 101–119. https://doi.org/10.1159/000071150

Di Stefano, C., Rinaldesi, M., Quinquinio, C., Ridolfi, C., Vallasciani, M., Sturiale, C., & Piperno, R. (2016). Neuropsychological changes and cranioplasty: A group analysis. *Brain Injury*, *30*, 164–171. https://doi.org/10.3109/02699052.2015.1090013

Fagerlund, S., Hupa, L., & Hupa, M. (2013). Dissolution patterns of biocompatible glasses in. 2-amino-2-hydoxymethyl-propane-1,3-diol (Tris) buffer. *Acta Biomaterialia*, *9*(2), 5400–5410. https://doi.org/10.1016/j.actbio.2012.08.051

Frantzen, J., Rantakokko, J., Aro, H., Heinanen, J., Kajander, S., Gullichsen, E., … Lindfors, N. C. (2011). Instrumented spondylodesis in degenerative spondylolisthesis with bioactive glass and autologous bone. A prospective 11-year follow-up. *J Spinal Disorders Techn*, *24*(7), 455–461. https://doi.org/10.1097/BSD.0b013e31822a20c6

Jiang, J., Lichtler, A. C., Gronowicz, G. A., Adams, D. J., Clark, S. H., Rosen, C. J., & Kream, B. E. (2006). Transgenic mice with osteoblast-targeted insulin-like growth factor-I show increased bone remodeling. *Bone*, *39*, 494–504. https://doi.org/10.1016/j.bone.2006.02.068

Kahles, F., Findeisen, H. M., & Bruemmer, D. S. (2014). Osteopontin: A novel regulator at the cross roads of inflammation, obesity and diabetes. *Mol Metab*, *3*(4), 384–393.

Kankare, J., & Lindfors, N. (2016). Reconstruction of vertebral bone defects suing an expandable replacement device and bioactive glass S53P4 in the treatment of vertebral osteomyelitis: Three patients and three pathogens. *Scandinavian Journal of Surgery*, *105*(4), 248–253. https://doi.org/10.1177/1457496915626834

Kasir, R., Vernekar, V. N., & Laurencin, C. T. (2017). Inductive biomaterials for bone regeneration. *Journal of Materials Research*, *32*(6), 1047–1060. https://doi.org/10.1557/jmr.2017.39

Kusuyama, J., Bandow, K., Ohnishi, T., Hisadome, M., Shima, K., Semba, I., & Matsuguchi, T. (2017). Osteopontin inhibits osteoblast responsiveness through the down-regulation of focal adhesion kinase mediated by the induction of low-molecular weight protein tyrosine phosphatase. *Mol Biol Cell*, *28*(190), 1326–1336.

LeGeros, R. Z. (2002). Properties of osteoconductive biomaterials: Calcium phosphates. *Clin Ortop Relat Res*, *395*, 81–98. https://doi.org/10.1097/00003086-200202000-00009

Mehrara, B., Most, D., Chang, J., Bresnick, S., Turk, A., Schendel, S., … Longaker, M. (1999). Basic fibroblast growth factor and transforming growth factor B-1 expression in the developing dura mater correlates with calvarial bone formation. *Plastic Reconstr Surg*, *104*(2), 435–444. https://doi.org/10.1097/00006534-199908000-00017

Monfoulet, L. E., Becquart, P., Marchat, D., Vandamme, K., Bourguignon, M., Pacard, E., … Logeart-Avramoglou, D. (2014). The pH in the microenvironment of human mesenchymal stem cells is a critical factor for optimal osteogenesis in tissue-engineered constructs. *Tissue Engineering. Part a*, *20*(13–14), 1827–1840. https://doi.org/10.1089/ten.tea.2013.0500

Nakamura, S., Matsumoto, T., Sasaki, J., Egusa, H., Lee, K. Y., Nakano, T., … Nakahiura, A. (2010). Effect of calcium ion concentrations on osteogenic differentiation and hematopoietic stem cell niche-related protein expression in osteoblasts. *Tissue Engineering. Part a*, *16*(8), 2467–2473. https://doi.org/10.1089/ten.tea.2009.0337

Nganga, S., Ylä-Soininmäki, A., Lassila, L. V. J., & Vallittu, P. K. (2011a). Interface shear strength and fracture behaviour of porous glass-fibre-reinforced composite implnat and bone model material. *Journal of the Mechanical Behavior of Biomedical Materials*, *4*, 1797–1804. https://doi.org/10.1016/j.jmbbm.2011.05.037

Nganga, S., Ylä-Soininmäki, A., Lassila, L. V. J., & Vallittu, P. K. (2011b). Interface shear strength and fracture behavious of porous glass-fibre-reinforced composite implant and bonr model material. *Journal of the Mechanical Behavior of Biomedical Materials*, *4*, 1797–1804. https://doi.org/10.1016/j.jmbbm.2011.05.037

Nganga, S., Zhang, D., Moritz, N., Vallittu, P. K., & Hupa, L. (2012a). Multilayer porous fiber-reinforced composites for implants: in vitro calcium phosphate formation in the presence of bioactive glass. *Dental Materials*, *28*, 1134–1145. https://doi.org/10.1016/j.dental.2012.08.005

Nganga, S., Zhang, D., Moritz, N., Vallittu, P. K., & Hupa, L. (2012b). Multlayer porous fiber-reinforced composites for implants: in vitro calcium phosphate formation in the presence of bioactive glass. *Dental Materials*, *28*, 1134–1145. https://doi.org/10.1016/j.dental.2012.08.005

Oliver-De La Cruz, J., Nardone, G., Vrbsky, J., Pompeiano, A., Perestrelo, A. R., Capradossi, F., … Forte, G. (2019). Substrate mechanics controls adipogenesis through YAP phosphorylation by dictating cell spreading. *Biomaterials*, *205*, 64–80.

Peltola, M., Vallittu, P. K., Vuorinen, V., Aho, A., Puntala, A., & Aitasalo, K. (2012). Novel composite implant in craniofacial bone reconstruction. *Eur Arch Otorinolryngol*, *269*, 623–628. https://doi.org/10.1007/s00405-011-1607-x

Piitulainen, J., Posti, J. P., Vallittu, P. K., Aitasalo, K., & Serlo, W. (2019). A large calvarial bone defect in a child: Osseointegration of an implant. *World Neurosurgery*, *124*, 282–286. https://doi.org/10.1016/j.wneu.2019.01.028

Piitulainen, J. M., Kauko, T., Aitasalo, K. M. J., Vuorinen, V., Vallittu, P. K., & Posti, J. P. (2015). Outcomes of cranioplasty with synthetic materials and autologous bone grafts. *World Neurosurgery*, *83*, 708–714. https://doi.org/10.1016/j.wneu.2015.01.014

Porgham Daryasari, M., Dusti Telgerd, M., Hossein Karami, M., Zandi-Karimi, A., Akbarijavar, H., Khoob, I. M., … Sadat, M. F. (2019). Poly-l-lactic acid scaffolds incorporated chitosan coated mesoporous silica nanoparticles as pH-sensitive composite for enhanced osteogenic differentiation of human adipose tissue stem cells by dexamethasone delivery. *Artif Cells Nanomed Biotechnol*, *47*(1), 4020–4029. https://doi.org/10.1080/21691401.2019.1658594

Posti, J. P., Piitulainen, J. M., Hupa, L., Fagerholm, S., Frantzen, J., Aitasalo, K. M. J., … Vallittu, P. K. (2015). Fiber-reinforced composite-bioactive glass cranioplasty implant: A case report of an early development stage implant. *Journal of the Mechanical Behavior of Biomedical Materials*, *55*, 191–200. https://doi.org/10.1016/j.jmbbm.2015.10.030

Ramesh, S., Tan, C. Y., Hamdi, M., Sopyan, I., & Teng, W. D. (2004). The influence of Ca/P ratio on the propertuies of hydroxyapatite bioceramics. *Proc of SPIE*, *6423*. https://doi.org/10.1117/12.779890

Rantakokko, J., Frantzen, J. P., Heinanen, J., Kajander, S., Kotilainen, E., Gullichsen, E., & Lindfors, N. C. (2012). Posterolateral spondylodesis using bioactive glass S53P4 and autogenous bone in instrumented unstable lumbar spine burst fractures. *Scandinavian Journal of Surgery*, *101*(1), 66–71. https://doi.org/10.1177/145749691210100113

Rendenbach C, Schöllen M, Bueschel J, Gauer T, Vallittu PK, Seöacik J, Kutzner D, Heiland M, Smeets R, Fiehler J, Simonsen S. n.d. Evaluation and reduction of magnetic resonance imaging artifacts induced by distinct plates for osseous fixation. An in vitro study @3T. Dentomaxillofac Radiol 2018;May;23:20170361. Doi: 10.1259/dmfr.20170361.

Sarin, J., Björkvik, L., Hiltunen, M., Hupa, L., Pulkkinen, J., & Vallitttu, P. K. (2016). The effect of fibrin sealant on bioactive glass S53P4 particles—pH impact and dissolution characteristics in vitro. *J Sci Adv Mater Devices*, *1*, 482–487. https://doi.org/10.1016/j.jsamd.2016.10.006

Sautier, J. M., Kokubo, T., Ohtsuki, T., Nefussi, J. R., Boulekbache, H., Oboeuf, M., … Forest, N. (1994). Bioactive glass-ceramic containing crystalline apatite and wollastonite initiates biomineralization in bone cell cultures. *Calcified Tissue Int*, *55*(6), 458–466. https://doi.org/10.1007/BF00298560

Schäck, L. M., Noack, S., Winkler, R., Wissmann, G., Behrens, P., Wellmann, M., … Hoffmann, A. (2013). The phosphate source influences gene expression and quality of mineralization during in vitro osteogenic differentiation of human mesenchymal stem cells. *PLoS ONE*, *8*(6), e65943, 1–12. https://doi.org/10.1371/journal.pone.0065943

Shih, Y.-U. R., Hwang, Y. S., Phadke, A., Kang, H., Hwang, N. S., Caro, E. J., … Varghese, S. (2014). Calcium phosphate-bearing matrices induce osteogenic differentiation of stem cells through adenosine signaling. *PNAS*, *111*(3), 990–995. https://doi.org/10.1073/pnas.1321717111

Shiu, H. T., Leung, P. C., & Ko, C. H. (2018). The roles of cellular and molecular components of a hematoma at earlky stage of bone healing. *J Tissue Eng Reg Med*, *12*(4), e1911–e1925. https://doi.org/10.1002/term.2622

Silver, I. A., Deas, J., & Erecinska, M. (2001). Interactions of bioactive glasses with osteoblasts in vitro: effects of 45S5 bioglass, and 58S and 77S bioactive glasses on metabolism, intracellular ion concentrations and cell viability. *Biomaterials*, *22*, 175–181. https://doi.org/10.1016/S0142-9612(00)00173-3

Storm, E. E., Huynh, T. V., Copeland, N. G., Jenkins, N. A., Kingsley, D. M., & Lee, S. J. (1994). Limb alterations in brachypodism mice due to mutations in a new member of the TGF beta-superfamily. *Nature*, *368*(6472), 639–643. https://doi.org/10.1038/368639a0

Szcesny, G. (2018). Fracture repairs: Its pathomechanism and disturbances. *Intech Open*, 3–22. https://doi.org/10.5772/intechopen.76252

Tan, J., Wang, D., Cao, H., Qiao, Y., Zhu, H., & Liu, X. (2018). Effect of local alkaline microenvironment on the behaviors of bacteria and osteogenic cells. *ACS Applied Materials & Interfaces*, *10*(49), 420–429.

Tuusa, S. M.-R., Lassila, L. V. J., Matinlinna, J. P., Peltola, M. J., & Vallittu, P. K. (2005). Initial adhesion of glass-fibre reinforced composite to surface of porcine calvarial bone. *J Biomed Mater Res – Part a*, *75*, 334–342.

Tuusa, S. M.-R., Peltola, M. J., Tirri, T., Lassila, L. V. J., & Vallittu, P. K. (2007 Jul). Frontal bone defect repair with experimental glass-fiber-reinforced composite with bioactive glass granule coating. *J Biomed Mater Res B Appl Biomater*, *82*(1), 149–155.

Tuusa, S. M.-R., Peltola, M. J., Tirri, T., Puska, M. A., Röyttä, M., Aho, H., … Vallittu, P. K. (2008). Reconstruction of critical size calvarial bone defect in rabbits with glass-fiber-reinforced composite with bioactive glass granule coating. *Journal of Biomedical Materials Research. Part B, Applied Biomaterials*, *84*, 510–519. https://doi.org/10.1002/jbm.b.30898

Väkiparta, M., Forsback, A.-P., Lassila, L. V., Jokinen, M., Yli-Urpo, A. U. O., & Vallittu, P. K. (2005). Biomimetic mineralization of partially bioresorbable glass fiber reinforced composite. *Journal of Materials Science. Materials in Medicine*, *16*, 873–879. https://doi.org/10.1007/s10856-005-3576-3

Vallittu, P. K. (2017). Bioactive glass in cranial implants—An overview. *Journal of Materials Science*, *52*(15), 8772–8784. https://doi.org/10.1007/s10853-017-0888-x

Vallittu, P. K., Närhi TO, & Hupa, L. (2015). Fiber glass—Bioactive glass implants. *Review. Dent Mater*, *31*, 371–381. https://doi.org/10.1016/j.dental.2015.01.003

Viti, F., Landini, M., Mezzelani, A., Petecchia, L., Milanesi, L., & Scaglione, S. (2016). Osteogenic differentiation of MSC through calcium signaling activation: Transcriptomics and functional analysis. *PLoS ONE*, *11*(2), e0148173, 1–21. https://doi.org/10.1371/journal.pone.0148173

Wang, R. N., Green, J., Wang, Z., Deng, Y., Qiao, M., Peabody, M., … Shi, L. L. (2014). Bone morphogenetic protein (BMP) signaling in development and human diseases. *Genes Dis*, *1*(1), 87–105. https://doi.org/10.1016/j.gendis.2014.07.005

Zanotti, B., Zingaretti, N., Verlicchi, A., Robiony, M., Alfieri, A., & Parodi, P. C. (2016). Cranioplasty: Review of materials. *The Journal of Craniofacial Surgery*, *27*(8), 20161–22072.

Zhang, D., Hupa, M., & Hupa, L. (2008). In situ pH within particle beds of bioactive glasses. *Acta Biomaterialia*, *4*(5), 1498–1505. https://doi.org/10.1016/j.actbio.2008.04.007

Zhang, D., Lepparanta, O., Munukka, E., Ylanen, H., Viljanen, M. K. L., Eerola, E., … Hupa, L. (2010). Antimicrobial effects and dissolution behavior of six bioactive glasses. *Journal of Biomedial Materials Research Part a*, *93A*(2), 475–483.

SUPPORTING INFORMATION

Additional supporting information may be found online in the Supporting Information section at the end of this article.

Data S1. Supporting information S1

Figure S1. Supporting information

How to cite this article: Vallittu PK, Posti JP, Piitulainen JM, et al. Biomaterial and implant induced ossification: in vitro and in vivo findings. *J Tissue Eng Regen Med*. 2020;14:1157–1168. https://doi.org/10.1002/term.3056